

BIOSCAN-CLIP: Bridging Vision and Genomics for Biodiversity Monitoring at Scale

ZeMing Gong¹ Austin T. Wang¹ Joakim Bruslund Haurum² Scott C. Lowe³
Graham W. Taylor^{3,4} Angel X. Chang^{1,5}

Simon Fraser University¹ Aalborg University² Vector Institute³ University of Guelph⁴ Amii⁵

{zmgong, atw7, angelx}@sfu.ca, {joha}@create.aau.dk,
{scott.lowe}@vectorinstitute.ai, {gwtaylor}@uoguelph.ca
<https://3dlg-hcvc.github.io/bioscan-clip/>

Abstract

Measuring biodiversity is crucial for understanding ecosystem health. While prior works have developed machine learning models for taxonomic classification of photographic images and DNA separately, in this work, we introduce a multimodal approach combining both, using CLIP-style contrastive learning to align images, DNA barcodes, and textual data in a unified embedding space. This allows for accurate classification of both known and unknown insect species without task-specific fine-tuning, leveraging contrastive learning for the first time to fuse DNA and image data. Our method surpasses previous single-modality approaches in accuracy by over 11% on zero-shot learning tasks, showcasing its effectiveness in biodiversity studies.

1. Introduction

As environmental change and habitation loss accelerate, monitoring biodiversity is crucial to understand and maintain the health of ecosystems. Taxonomic classification of organisms at scale is especially important for understanding regional biodiversity and studying species interactions.

Recently, computer vision techniques have been used to classify species observed in images [17, 40, 58, 60] including for ecological monitoring [11]. However, relying solely on images for identifying and classifying organisms fails to consider the rich evolutionary relationship between species and may miss fine-grained species differences. To better capture these distinctions, researchers have used DNA sequences for tasks such as genome understanding and taxonomic classification [3, 8, 26, 42, 66]. In particular, DNA barcodes [23], small sections of DNA from specific genes such as the COI gene [38] in mitochondrial DNA, are useful for species identification [3]. However, collecting DNA requires specialized equipment and is more expensive and less

accessible than images. A desirable approach is to use approaches that leverage DNA information at training time but only need images of new specimens at inference time [5].

Machine learning advances have made it possible to combine information from different modalities. For instance, CLIP [47] used contrastive learning to encode text (e.g., “cat”) and images (e.g., a photo of a cat) into a common space for zero-shot classification. A recent model BioCLIP [52] aligned images of organisms with common names and taxonomic descriptions to classify plants, animals, and fungi. Most prior work only uses a subset of modalities (image only [17, 58, 60], DNA only [3, 8, 26, 42, 66], text and image [52]) rather than combining information from images, text, and DNA barcodes. They also often require a text description or complete taxonomic annotations, which are expensive and time-consuming to obtain.

In this work, we propose BIOSCAN-CLIP which uses contrastive learning to map biological images, textual taxonomic labels, and DNA barcodes to the same latent space. With this aligned space, we do not need comprehensive or noise-free taxonomic annotations. We flexibly take either images or DNA barcodes as input to predict the taxonomy. Our embedding space also enables future research leveraging multiple modalities to examine commonalities and differences between species. Aside from ecological benefits, building such a foundation model for biodiversity provides a case study of broader challenges in identifying fine-grained differences, both visually and textually. Visual differences between species are often subtle, and the DNA and taxonomic labels do not have much semantic overlap with everyday natural language. Thus, tokens for DNA and text from taxonomic labels are different from tokens typically found in large language models trained on internet data. We showcase the benefits of pretraining with all three modalities through improved taxonomic classification accuracy over prior works in both retrieval and zero-shot settings.

2. Related Work

We review work on pretraining multimodal models on images, DNA, and text, including foundation models and multimodal learning with fine-grained images and their application in biological problems.

2.1. Fine-grained multimodal learning

Recent work on vision and language addresses the challenge of distinguishing between highly similar categories [22, 51]. Radford et al. [47] showcased how natural language supervision can significantly improve visual models. Contrastive learning on over 400 million pairs of images and text enabled matching multi-modal data and zero-shot transfer across diverse tasks. Later work built on this architecture to improve the embedding space [9, 16, 20, 27, 34, 62] or implement support for generation tasks [31–33]. Wei et al. [60] provide a comprehensive survey on deep learning for fine-grained image analysis. Recent works train domain-specific foundation models on large corpora of image or natural language datasets, leveraging similar architectures and training strategies [10, 21, 52]. Other approaches extend the multimodal architecture to more than two modalities, including audio, video, or 3D representations [1, 2, 19, 39, 45, 49, 63]. We demonstrate the value of applying similar strategies for pretraining foundation models to the problem of biodiversity monitoring.

2.2. Models for DNA and biological images

There is much work on machine learning for DNA data, especially in genome understanding [4, 29, 30, 35]. Recently, there is increasing interest in developing foundation models of DNA sequences [3, 8, 13, 26, 43, 55, 66, 67]. Many of these works leverage transformer architectures and self-supervised learning techniques such as masked language modeling [14] to pretrain models on large DNA datasets for downstream genome analysis tasks such as promoter prediction or metagenomics binning [3, 26, 66, 67]. Zhou et al. [67] incorporate curriculum-based contrastive learning to learn a “species-aware” embedding space for DNA. Other work explored using DNA data for taxonomic classification [3, 36, 42]. BERTax [42] pretrained a BERT [14] model for hierarchical taxonomic classification. However, they focused on superkingdom, phylum, and genus classification, which are coarser-grained categories and thus easier than classifying species. BarcodeBERT [3] showed that models pretrained on DNA barcodes, rather than general DNA datasets, can be particularly effective for taxonomic classification. Our work extends these models for encoding DNA by learning a shared embedding space with images and text as well, addressing issues with the cost of obtaining DNA data in practice by allowing for cross-modal image queries.

There is also work on taxonomic classification based on images of plant, bird, and insect species [7, 46, 58].

Methods for coarse supervision help learn fine-grained taxonomic categories, given the number and rarity of species [48, 54, 56]. Contrastive learning has been used to better differentiate between fine-grained species characteristics [12, 61]. However, species differences are not necessarily easily detectable by visual cues alone. To that end, we leverage DNA data in addition to images to classify species, while still preserving the benefits of the relative ease of acquiring visual data of new organisms.

2.3. Multimodal models for biology

Prior works explored building pretrained models based on only images or DNA, and largely relied on fine-tuning classifiers on a set of known species. This limits those approaches to a closed set of species, whereas we are concerned with being able to identify unseen species, i.e. those for which we have no examples in the modality of interest. Furthermore, these works are limited to single modalities. Recent works have begun building multimodal models for biological applications [25, 37, 64], including several works in taxonomic classification [5, 6, 44, 52]. Nguyen et al. [44] introduced Insect-1M, a large-scale dataset with images annotated with their taxonomic levels (from class to species) and dense text descriptions. Their method applied contrastive learning across text and image modalities with a patch-based attention to build an “insect foundation” model. BioCLIP [52] applied multimodal contrastive pretraining on images and text descriptions to a larger scale, collecting multiple datasets into the TreeOfLife-10M dataset. While achieving impressive results, these models and datasets only consider images and text, thus being more limited with new species, in which taxonomic labels are not available for alignment. They do not take advantage of the rich taxonomic knowledge available in sources like the Barcode of Life Datasystem (BOLD), that at the time of writing is approaching 15 M validated DNA barcodes, most of which have associated expert-assigned taxonomic labels.

Badirli et al. [5] employed a Bayesian zero-shot learning approach using DNA to model priors for species classification by image. They relate unseen species to nearby seen species in the DNA embedding space, given barcode data for both, in order to construct Gaussian priors by which to classify images. Badirli et al. [6] employ similar Bayesian techniques and combine image and DNA embeddings in the same space to predicting the genus for unseen species, assuming that genera are largely already discovered. While this approach learns to project between embedding spaces of different modalities, the alignment is not end-to-end optimized, limiting the amount of alignment which can be obtained. We show that taking this BZSL approach and using our aligned embedding space of image and DNA learned using a contrastive loss, we can have a more accurate model. By incorporating text into our model during pretraining, we

can also leverage taxonomic annotations more explicitly, when available, without relying on their presence.

3. Method

To align representations of images, DNA barcodes, and taxonomy labels as text, we start with pretrained encoders for each modality and then apply LoRA finetuning [24] with a multimodal contrastive loss (see Figure 1). During inference, we use our fine-tuned encoders to extract features for a *query* image and match against a database of image and DNA embeddings (*keys*) for which the taxonomic information is already known. To classify the query image, we take the taxonomic information associated with the most closely matched key. While we can also query against the taxonomies themselves, the labels may be incomplete or unknown. Thus, images and DNA barcodes comprise a more robust and defining set of records against which to query.

3.1. Training

Contrastive learning. We base our approach on a contrastive learning scheme similar to CLIP [47], which uses large-scale pretraining to learn joint embeddings of images and text. In contrastive learning, embeddings for paired samples are pulled together while non-paired samples are pushed apart, thus aligning the semantic spaces for cross-modal retrieval. Following prior work [49], we extend CLIP [47] to three modalities by considering the modalities in pairs with the NT-Xent loss [50] between two modalities to align their representations. Let matrices \mathbf{X} , \mathbf{D} , and \mathbf{T} represent the batch of ℓ_2 -normalized embeddings of the image, DNA, and text modalities. The i -th row of each corresponds to the same instance corresponding to a physical specimen, thus rows X_i and D_i are features from the same sample, forming a positive pair. Features in different rows X_i and D_j , $i \neq j$, come from different samples and are negative pairs. The contrastive loss for pair i is

$$L_i^{(X \rightarrow D)} = -\log \frac{\exp(X_i^T D_i / \tau)}{\sum_{k=1}^n \exp(X_i^T D_k / \tau)},$$

$$L_i^{(D \rightarrow X)} = -\log \frac{\exp(D_i^T X_i / \tau)}{\sum_{k=1}^n \exp(D_i^T X_k / \tau)}$$

$$L_{XD} = \sum_{i=1}^n (L_i^{(X \rightarrow D)} + L_i^{(D \rightarrow X)})$$

where $\tau = 0.07$ is a fixed temperature, based on the initial value used in [47]. We apply the loss symmetrically to normalize over the possible paired embeddings for each modality [49, 65]. We repeat this for each pair of modalities and sum them to get the final loss, $L = L_{XD} + L_{DT} + L_{XT}$.

Pretrained encoders. For each data-modality, we a pretrained model to initialize our encoders. *Images*: we use

a ViT-B network¹ pretrained on ImageNet-21k and finetuned on ImageNet-1k [15]. *DNA barcodes*: we use BarcodeBERT [3] with 5-mer tokenization, pretrained on about 893K DNA barcodes using masked language modelling. The training data for BarcodeBERT is highly similar to the DNA barcodes in the BIOSCAN-1M dataset making it ideal for our study. *Text*: we use the pretrained BERT-small introduced by Turc et al. [57] to encode taxonomic labels.

Low-rank adaptation. To efficiently fine-tune the pretrained transformer models, we apply Low-Rank Adaptation (LoRA) [24], a method for fine-tuning large neural network models that greatly reduces the number of trainable parameters. For our LoRA implementation, we add an additional low-rank residual layer to the query and key projectors of each attention module. The projectors thus take the form $W_{\text{LoRA}} = W + W_i W_o$, where $W \in R^{i \times o}$ represents the frozen parameters of the pretrained weights from the projector, whilst $W_i \in R^{i \times r}$ and $W_o \in R^{r \times o}$ represent the added low-rank weights. By choosing a rank r much smaller than the input and output dimensions i and o , fewer parameters need to be updated with LoRA than with the original layer ($ir + ro \ll io$).

By using LoRA, we are able to train with less parameters and less memory, allowing us to train with larger batch sizes on limited resources. This is especially important for contrastive learning as increasing the batch size allows for more positive and negative pairs when calculating the contrastive loss, and thereby improves learning effectiveness. Experimentally, LoRA reduces the number of trainable parameters from 203M to 1.9M. With batch size 400, the model requires just 71.5GB, allowing us to train on an A100 with 80GB, which would be infeasible without LoRA.

3.2. Inference

To use the model for predicting taxonomic labels, we calculate the cosine similarity between the embedded input image (*query*) and reference image or DNA embeddings (*keys*) sampled from available species. We take the taxonomic label (order, family, genus, species) associated with the closest key as the prediction. This method allows us to evaluate our model in a zero-shot setting on species which were not seen by the model during the LoRA fine-tuning, as it is not constrained to predict within a fixed set of classes. The embedding space also gives us the flexibility to use the representation in other downstream models, such as a supervised classifier or a Bayesian model similar to [5, 6].

4. Task and data

To evaluate our method, we perform taxonomic classification given an input image. The input is a biological image (query) along with a reference set of labelled DNA

¹Loaded as `vit_base_patch16_224` in the `timm` library.

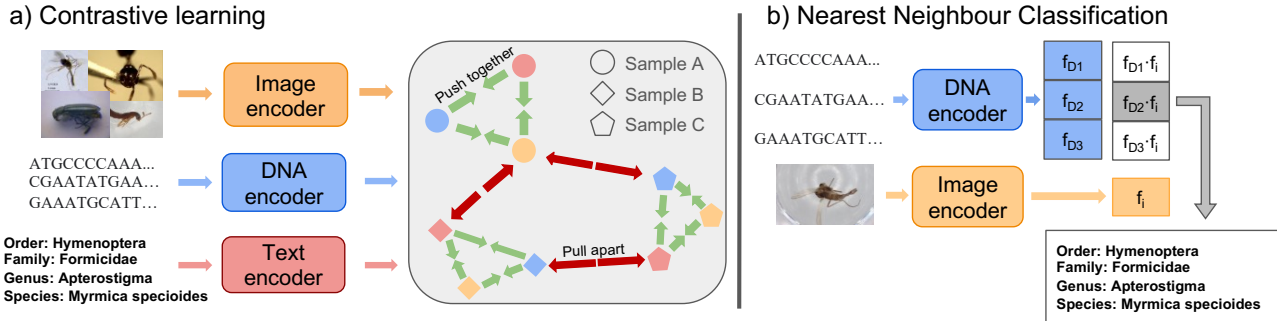


Figure 1. *Overview of BIOSCAN-CLIP.* (a) Our model consists of three encoders for processing images, DNA barcodes, and text. During training, we use a contrastive loss to align the image, DNA, and text embeddings. (b) At inference time, we embed a *query* image and match it to a database of existing image and DNA embeddings (*keys*). We use cosine similarity to find the closest key embedding and use its taxonomic label to classify the query image.

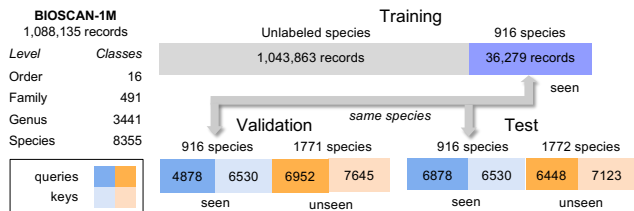


Figure 2. *Data partitioning.* We split the BIOSCAN-1M data into training, validation, and test partitions. The training set (used for contrastive learning) has records without any species labels as well as a set of *seen* species. The validation and test sets include *seen* and *unseen* (not seen during training) species. These images are further split into subpartitions of *queries* and *keys* for evaluation.

barcodes, other labelled biological images (key), or known taxonomic labels encoded as text (as demonstrated in Table 5). We match the input feature with the closest neighbours in a database using aligned representations and assess accuracy across taxonomic levels by averaging over samples and taxon classes. The predictions are evaluated at each taxonomic level by averaging accuracy over samples (micro) and taxon classes (macro). Unlike basic fine-tuning with a fully connected layer, our approach identifies unseen species using images or DNA without knowing all potential species upfront. Instead, we use reference features for taxonomic prediction or novel class identification. We split our data so that some species are “unseen” during training, and report prediction accuracy for both seen and unseen species to study model generalization.

Dataset. We use the BIOSCAN-1M dataset [18], a curated collection of over one million insect data records. Each record in the dataset includes a high-quality insect image, expert-annotated taxonomic label, and a DNA barcode. However, the dataset has incomplete taxonomic labels, with fewer than 10% of records labelled at the species level. This poses a challenge for conventional supervised methods, which would require species-level annotations, but our method is able to flexibly leverage partial or missing taxo-

omic information during contrastive learning. The dataset also possesses a long-tailed class imbalance, typical of real-world biological data, presenting a challenge for modelling. Given the vast biodiversity of insects, with an estimated 80% undescribed [53], and the necessity to discern subtle visual differences, this dataset offers a significant challenge and opportunity for our model.

Data partitioning. We split BIOSCAN-1M into train, validation, and test sets to evaluate zero-shot classification capabilities and model generalization to unseen species. Records for well-represented species (at least 9 records) are partitioned at an 80/20 ratio into seen and unseen, with seen records allocated to each of the splits and unseen records allocated to validation and test. All records without species labels are used in contrastive pretraining, and any species with 2–8 records are added evenly to the *unseen* splits in the validation and test sets. Importantly, we ensure that any *unseen* species are mutually exclusive between the validation and test sets and likewise do not overlap with *seen* species for labeled records. Finally, among each of the seen and unseen sub-splits within the validation and test sets, we allocate equal proportions of records as *queries*, to be used as inputs during evaluation, and *keys*, to be used as our reference database. See Figure 2 for split statistics and Appendix A for further details.

Data preprocessing. During inference, we resized images to 256×256 and applied a 224×224 center crop. For the DNA input, following Arias et al. [3], we set a maximum length of 660 for each sequence and tokenized the input into non-overlapping 5-mers. Finally, similar to Stevens et al. [52], we concatenated the taxonomic levels of the insects together as text input. As we did not have the common names of each record, we used the order, family, genus, and species, up to known labels. With this approach, we can still provide the model with knowledge of the higher-level taxonomy, even if some records do not have species-level annotations.

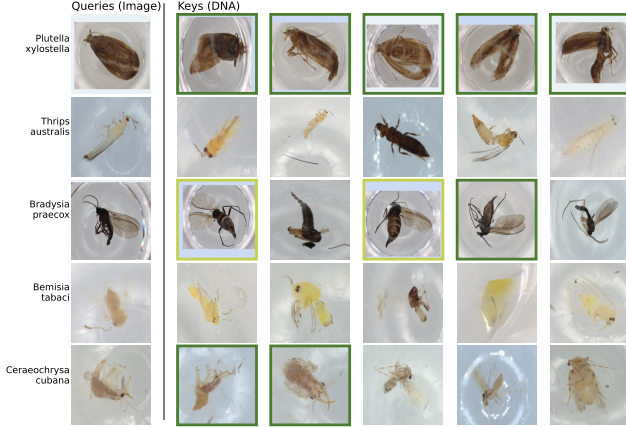


Figure 3. Example image query-key pairs. For five distinct query images, we show the top-5 nearest specimens from the validation-key dataset retrieved based on the cosine-similarity between the image query and DNA keys. Surrounding boxes denote keys of the same species (green) or same genus (yellow) as the query.

5. Experiments

We study the model’s ability to retrieve taxonomic labels using images in the BIOSCAN-1M dataset [18] of species that were either *seen* or *unseen* during contrastive learning. We also experiment on the INSECT dataset [5] for Bayesian zero-shot learning (BZSL) species classification. We report the top-1 accuracy for the *seen* and *unseen* splits, as well as their harmonic mean (H.M.). In the main paper, we focus on evaluation on the validation set using image embeddings as queries as images are the most readily available modality. In the appendices, we provide full results on both the validation and test set (Appendix B.1), experiments that query with DNA features (Appendix B.2), and visualization of the aligned embedding space (Appendix B.3).

5.1. Retrieval by image query

We conducted experiments on BIOSCAN-1M [18] to study whether taxonomic classification accuracy improves with contrastive learning, particularly with the inclusion of DNA barcodes as an additional modality. We compare trained aligned embedding spaces with different combinations of modalities: image (I), DNA (D), and text (T). Figure 3 shows retrieval examples using image queries and DNA keys from our full model (aligning I+D+T), for which the retrieval is successful if the DNA’s taxonomy matched the image’s. These examples show similarity between query and retrieved images across taxa, suggesting effective DNA and image embedding alignment despite differences in insect orientation and placement.

Implementation details. For our experiments, models were trained on two 80GB A100 GPUs for 15 epochs with a total batch size of 800, using the Adam optimizer [28] with a learning rate of 0.001.

Table 1. Top-1 accuracy (%) on the validation set for different combinations of aligned embeddings (image, DNA, text) during contrastive training. We use **images** as queries and **DNA** as keys during inference. When aligning embeddings with text, we use a concatenation of the word representation of taxonomic levels. As a baseline, we show the results prior to contrastive learning (no alignment). We report the accuracy for seen and unseen species, and the harmonic mean (H.M.) between these (bold: highest acc.).

| Taxon | Aligned embeddings | | | Micro top-1 acc | | | Macro top-1 acc | | |
|---------|--------------------|-----|-----|-----------------|-------------|-------------|-----------------|-------------|-------------|
| | Img | DNA | Txt | Seen | Unseen | H.M. | Seen | Unseen | H.M. |
| Order | × | × | × | 41.3 | 38.3 | 39.7 | 12.8 | 8.7 | 10.4 |
| | ✓ | ✓ | × | 98.5 | 97.6 | 98.0 | 87.4 | 52.6 | 68.7 |
| | ✓ | ✓ | ✓ | 98.7 | 97.6 | 98.2 | 98.3 | 58.8 | 73.2 |
| Family | × | × | × | 3.3 | 4.8 | 3.9 | 1.1 | 0.7 | 0.9 |
| | ✓ | ✓ | × | 80.4 | 74.0 | 77.1 | 50.4 | 28.3 | 36.2 |
| | ✓ | ✓ | ✓ | 84.6 | 79.0 | 81.7 | 56.3 | 35.2 | 43.3 |
| Genus | × | × | × | 0.9 | 3.1 | 1.4 | 0.1 | 0.1 | 0.1 |
| | ✓ | ✓ | × | 52.2 | 37.0 | 43.3 | 24.7 | 7.9 | 12.0 |
| | ✓ | ✓ | ✓ | 58.5 | 43.5 | 49.9 | 30.1 | 11.7 | 16.9 |
| Species | × | × | × | 0.0 | 2.0 | 0.0 | 0.0 | 0.0 | 0.0 |
| | ✓ | ✓ | × | 37.5 | 17.1 | 23.5 | 15.6 | 2.5 | 4.3 |
| | ✓ | ✓ | ✓ | 42.0 | 30.1 | 35.1 | 17.4 | 3.9 | 6.4 |

Taxonomic classification. In Table 1, we report the top-1 accuracy on the BIOSCAN-1M validation set, averaged over samples (micro) and over species (macro) for seen and unseen species. Without any alignment, the cross-modal retrieval performance from image to DNA is effectively at chance accuracy, scoring extremely low for levels more fine-grained than order. Contrastive learning improves performance on all metrics, with the highest accuracy achieved when training with all three modalities (I+D+T), demonstrating the value of aligning to a shared embedding space. The performance gain of incorporating text shows the utility of embedding the available taxonomic labels. While this approach does leverage taxonomic annotations, we do not require them to be comprehensive.

Since we use DNA features as keys, we focus on experiments which included the DNA encoder (see Appendix B.1 for more complete results). As expected, the performance drops for more specific taxa (e.g. accuracy for order is much higher than for species), due to both the increased number of labelling options and the more fine-grained differences between them. When we consider unseen species, there is a drop in performance compared to seen species, suggesting the model’s ability to generalize could be improved.

Micro-accuracy is also much higher than macro-accuracy, due to the skew in per-class accuracy toward more well-represented classes. These are easier to match correctly, as the seen species are observed more frequently during training, and a higher fraction of the keys bear the correct DNA barcode to the corresponding query. This imbalance reflects a broader issue in biodiversity science, where oversampling is prevalent, leading to a considerable skew or long-tail distribution in global databases. Figure 4 illustrates this trend in which common species tend to have

Table 2. Top-1 accuracy (%) on the validation set using images as queries and different key modalities for inference. We evaluate BIOSCAN-CLIP trained on all three modalities. We consider image features, DNA features, and the average of the two as *keys*, highlighting the best key method per taxon in bold.

| Taxon | Micro top-1 accuracy | | | | | | Macro top-1 accuracy | | | | | |
|---------|----------------------|------|-------------|-------------|------|------|----------------------|------|-------------|-------------|------|------|
| | Seen | | | Unseen | | | Seen | | | Unseen | | |
| | Image | DNA | Avg | Image | DNA | Avg | Image | DNA | Avg | Image | DNA | Avg |
| Order | 99.3 | 98.7 | 99.3 | 99.2 | 97.6 | 98.7 | 98.0 | 97.2 | 98.3 | 84.9 | 58.8 | 76.7 |
| Family | 90.5 | 84.6 | 91.7 | 89.1 | 79.0 | 86.2 | 80.1 | 56.3 | 78.0 | 65.6 | 35.2 | 58.0 |
| Genus | 74.8 | 58.5 | 76.9 | 73.4 | 43.5 | 64.0 | 57.0 | 30.1 | 56.2 | 46.0 | 11.7 | 35.0 |
| Species | 60.4 | 42.0 | 63.7 | 62.5 | 30.1 | 50.4 | 40.4 | 17.4 | 40.9 | 30.4 | 3.9 | 20.3 |

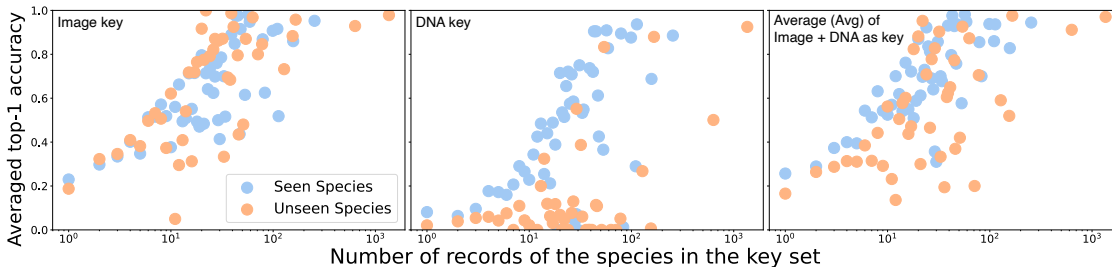


Figure 4. Average top-1 per-species accuracy, binned by count of species records in the key set, for different modalities as key. *Left*: using images as the key, the accuracy for both seen and unseen species increases as the number of records for the species in the key set rises. *Middle*: with DNA barcodes as the key, the accuracy of unseen species remains lower than seen species, even with the same number of records in the key set. *Right*: using the averaged image and DNA feature as the key, the accuracy for unseen species is typically slightly lower than that for seen species, even when the number of records in the key set is the same.

higher accuracy in all cases except unseen species, when using DNA barcodes as keys. This is likely due to the combined challenges of aligning modalities and generalizing to unseen species, such that the model is less able to map them appropriately in the embedding space.

Analysis of different keys. We use the aligned embedding space to assess the effectiveness of various key types—image alone, DNA alone, and their average—for image-based querying. By comparing how accuracy changes across modalities, we can better understand the degree to which data from various modalities are aligned within the latent space. We omit text as a key since we do not assume that we will have comprehensive taxonomic annotations at finer levels. Table 2 shows that querying against image keys almost always yields the highest 1-NN retrieval accuracy compared to DNA or average feature keys. When matching the image query features to DNA key features, there is a significant drop in accuracy at all taxonomic levels. This suggests that the model does not perfectly align the features across modalities. In certain cases for seen species, using the average of the image and DNA features increased the accuracy compared to either alone.

Combining image-image and image-DNA queries for improved ZSL. While using images as keys yields higher accuracy than DNA, images of unseen species are typically

Table 3. Accuracy (%) of predicting whether an image query corresponds to a seen or unseen species, as a binary classification problem (evaluated on the validation set). For the “DNA” strategy with Nearest Neighbour (NN), we use the nearest DNA feature to classify into seen or unseen. For the “IS+DU” strategy and NN, we threshold the highest cosine similarity score against image keys. For the supervised linear classifier (Linear), we threshold the confidence score of the prediction over seen species. We report accuracy for seen and unseen species, and their harmonic mean (H.M).

| Method | Strategy | Seen | Unseen | H.M. |
|-------------|----------|------|--------|-------------|
| NN (oracle) | DNA | 65.4 | 77.2 | 70.8 |
| NN | IS+DU | 67.3 | 72.9 | 69.9 |
| Linear | IS+DU | 49.3 | 87.5 | 63.1 |

not available in practice during deployment. This setting is similar to the zero-shot learning (ZSL) setting considered by Badirli et al. [5]. To tackle this setting, we consider a strategy (denoted IS+DU) to utilize the image embeddings for *seen* species, and DNA embeddings for *unseen* species.

We first frame the problem as an open-set recognition task [59] by using a classifier to determine whether a given image query corresponds to a *seen* species or an *unseen* species. In the first method, we utilize a 1-nearest neighbor (NN) classifier, and in the second, we use a supervised

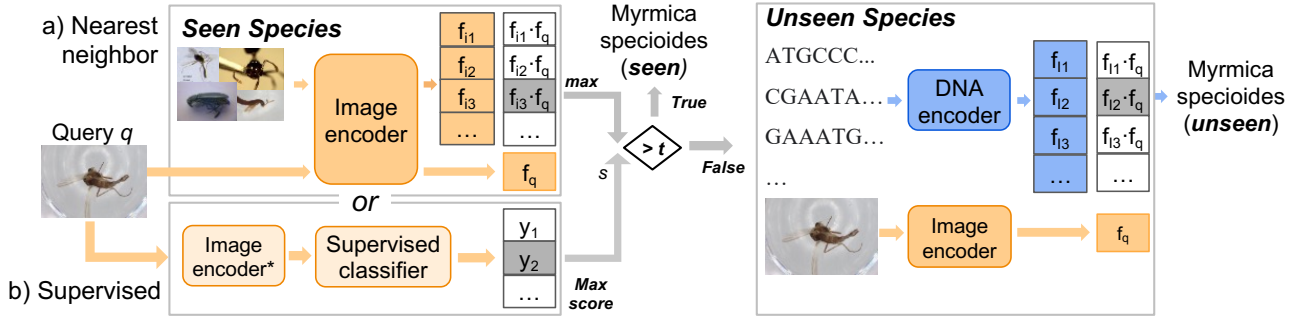


Figure 5. For cases where images of unseen species are not available, but we do have a set of DNA barcodes for unseen species, we can use a combination of image and DNA as key sets. We adapt BIOSCAN-CLIP for using images as keys for seen species and DNA for unseen species (i.e. the IS+DU strategy) to predict the species. Given an input image query q , we first classify it against seen species. The initial classifier can use: (a) a 1-NN approach thresholding the cosine similarity score $s = \max_k f_{ik} \cdot f_q$; or (b) a supervised classifier predicting over all seen species and thresholding the maximum softmax probability $s = \max y_k$ by threshold t . If $s < t$, we subsequently query with the image feature f_q using 1-NN with the DNA keys f_{ik} of the unseen species and predict the unseen species of the closest DNA feature. *During supervised classifier training, we also fine-tune the image encoder, only for use in the supervised pipeline.

Table 4. Top-1 accuracy (%) on the validation set using the Image+DNA+Text model with image query. We compare Nearest Neighbour using only DNA keys (NN DNA), vs. our two strategies to use Image key for seen and DNA key for Unseen, either NN or a supervised linear classifier. We also compare against BZSL [5] with our embeddings.

| Taxon | Method | Strategy | Micro top-1 acc | | | Macro top-1 acc | | |
|---------|--------|----------|-----------------|-------------|-------------|-----------------|-------------|-------------|
| | | | Seen | Unseen | H.M. | Seen | Unseen | H.M. |
| Order | NN | DNA | 98.7 | 97.6 | 98.2 | 97.2 | 58.8 | 73.2 |
| | NN | IS+DU | 98.9 | 97.9 | 98.4 | 97.2 | 55.6 | 70.7 |
| | Linear | IS+DU | 98.3 | 96.4 | 97.4 | 96.5 | 51.8 | 67.4 |
| | BZSL | IS+DU | 98.7 | 97.1 | 97.9 | 98.3 | 52.7 | 68.6 |
| Family | NN | DNA | 84.6 | 79.0 | 81.7 | 56.3 | 35.2 | 43.3 |
| | NN | IS+DU | 87.8 | 78.8 | 83.0 | 65.5 | 33.8 | 44.6 |
| | Linear | IS+DU | 86.4 | 75.5 | 80.6 | 61.2 | 29.7 | 40.0 |
| | BZSL | IS+DU | 89.6 | 75.3 | 81.9 | 80.7 | 28.0 | 41.5 |
| Genus | NN | DNA | 58.5 | 43.5 | 49.9 | 30.1 | 11.7 | 16.8 |
| | NN | IS+DU | 66.7 | 45.2 | 53.8 | 44.8 | 13.0 | 20.2 |
| | Linear | IS+DU | 61.1 | 43.3 | 50.7 | 35.5 | 10.9 | 16.7 |
| | BZSL | IS+DU | 65.4 | 40.7 | 50.2 | 54.2 | 10.8 | 18.0 |
| Species | NN | DNA | 42.0 | 30.1 | 35.1 | 17.4 | 3.9 | 6.4 |
| | NN | IS+DU | 52.0 | 30.0 | 38.0 | 32.0 | 4.3 | 7.6 |
| | Linear | IS+DU | 45.8 | 30.4 | 36.6 | 22.8 | 4.4 | 7.4 |
| | BZSL | IS+DU | 45.2 | 10.6 | 17.1 | 37.9 | 5.3 | 9.2 |

classifier fine-tuned with the image encoder (see Figure 5). For the NN classifier, we compute the cosine similarity of the image query features with the image features of the seen species. If the most similar image key has a similarity higher than threshold t_1 , it is classified as the species of the most similar key. Otherwise, we match the image query features with the DNA key features for unseen species. In the supervised fine-tuning approach, we add a linear classifier after the image encoder and fine-tune the encoder and classifier to predict the species out of the set of seen species. If the softmax probability exceeds t_2 , the image is classified as seen. Otherwise, the algorithm proceeds to the 1-NN strategy, using the DNA barcode features as keys. We tuned

t_1 and t_2 on the validation set using a uniform search over 1000 values between 0 and 1, maximizing the harmonic mean of the accuracy for seen and unseen species.

We first compare the ability of different methods to classify seen versus unseen species in the binary case. This allows us to tell whether we are effectively identifying whether a sample belongs to a seen or unseen species, without considering whether the species is correctly determined. Table 3 shows that our nearest neighbor combined approach (with the IS+DU strategy) performs best at identifying the seen species while having comparable accuracy in predicting *unseen* species. In these experiments, we use the I+D+T model with images as the queries. We use as an oracle the easier task of querying the seen and unseen DNA keys using 1-NN directly, without any initial classifiers.

Table 4 demonstrates the end-to-end performance of each strategy on the species classification task, assuming as before that we have access to DNA barcodes for the unseen species. We likewise find again that the NN method with the IS+DU strategy yielded the best accuracy in most taxa, especially improving performance at the genus and species level by several points. We also compare our simple ZSL strategy against a more sophisticated method, BZSL (see §5.3), at the species level. We find that BZSL with our embeddings is able to outperform our naive method on macro-level but underperforms on micro-accuracy, likely due to the large data skew of our dataset.

5.2. Comparison with BioCLIP

Next we compare our aligned embedding space with that of BioCLIP [52] by adapting their zero-shot learning demo script to perform species-level image classification. We use their pretrained model on the BIOSCAN-1M validation set, with image or text embeddings as keys. Keeping the experi-

Table 5. Species-level Top-1 accuracy (%) of using BioCLIP and our BIOSCAN-CLIP (BS-CLIP) on the validation set, using image embedding to match against different embeddings for retrieval (Image, DNA, and Text). We used the pretrained BioCLIP model, which was trained on TREEOFLIFE-10M, which combines multiple existing high-quality datasets such as iNat21 and BIOSCAN-1M. As its pretraining data includes BIOSCAN-1M and does not follow our splits, it may have also been trained on the unseen species.

| Model | Alignment | | | Micro top-1 accuracy | | | | | | | | | Macro top-1 accuracy | | | | | | | | |
|---------|-----------|-----|-----|----------------------|------|-------------|-------------|-------------|------------|-------------|------|------------|----------------------|------|-------------|--------|-----|------------|-------------|-----|-----|
| | | | | Seen | | | Unseen | | | H.M. | | | Seen | | | Unseen | | | H.M. | | |
| | Img | DNA | Txt | Img | DNA | Txt | Img | DNA | Txt | Img | DNA | Txt | Img | DNA | Txt | Img | DNA | Txt | Img | DNA | Txt |
| BioCLIP | ✓ | ✗ | ✓ | 37.7 | - | 4.5 | 48.1 | - | 4.1 | 42.2 | - | 4.3 | 21.1 | - | 4.5 | 15.6 | - | 3.5 | 17.9 | - | 3.9 |
| BS-CLIP | ✓ | ✗ | ✓ | 53.0 | - | 40.3 | 57.6 | - | 1.9 | 55.2 | - | 3.7 | 32.7 | - | 17.6 | 24.2 | - | 1.8 | 27.8 | - | 3.2 |
| BS-CLIP | ✓ | ✓ | ✓ | 60.4 | 42.0 | 50.1 | 62.5 | 30.1 | 2.1 | 61.4 | 35.1 | 4.1 | 40.4 | 17.4 | 22.4 | 30.4 | 3.9 | 2.2 | 34.7 | 6.4 | 3.9 |

mental setups almost identical, we compared BioCLIP with BIOSCAN-CLIP in Table 5. For BioCLIP, we combined the four concatenated taxonomic levels with their provided `openai_templates` as text input, while for BIOSCAN-CLIP, we used the concatenated labels only.

When using images as keys, BIOSCAN-CLIP consistently outperformed BioCLIP, even when BIOSCAN-CLIP was trained only on images and text. Since BioCLIP was trained on a much broader dataset, including but not limited to BIOSCAN-1M, it may have performed worse on insects as it was also trained on non-insect domains. BIOSCAN-CLIP can also leverage DNA features during inference, while BioCLIP is limited to image and text modalities.

When using text as keys, BIOSCAN-CLIP performed better than BioCLIP on seen species but marginally worse on unseen species. This is expected, as BIOSCAN-CLIP was not trained on the unseen species names, which we also would not know prior in practice. This illustrates that text typically does not perform well as keys and reinforces the benefit of using DNA in pretraining and inference.

5.3. Bayesian zero-shot learning

We also use our learned embeddings in Bayesian zero-shot learning (BZSL) [5] to show the benefit of our learned embeddings for species classification on the INSECT dataset [5], which contains 21,212 pairs of insect images and DNA barcodes from 1,213 species. We compare different combinations of image and DNA encoders. As baselines, we use a ResNet-101 image encoder, pretrained on ImageNet-1K (used in Badirli et al. [5]), and the ViT-B [15] image encoder, pretrained on ImageNet-21k and fine-tuned on ImageNet-1k. For DNA encoders, we evaluate the baseline CNN from Badirli et al. [5]; DNABERT-2 [66], a BERT-based model trained on multi-species DNA data; and BarcodeBERT [3], which was pretrained on arthropodic DNA barcode data.

Table 6 shows that using the baseline image encoder with BIOSCAN-CLIP-D surpasses all baseline methods in harmonic mean even without fine-tuning on the INSECT dataset, performing particularly better on unseen species. Furthermore, using BIOSCAN-CLIP-I improves performance in all metrics over the baseline image encoder, with

Table 6. Macro accuracy (%) for species classification in a Bayesian zero-shot learning task on the INSECT dataset. We compare several DNA encoders [3, 5, 66] to our own (BS-CLIP-D). We compare the baseline image encoder ResNet-101 used in [5] against our image encoder before (ViT-B) and after (BS-CLIP-I) pretraining on BIOSCAN-1M (BS-1M). We indicate the pretraining set for DNA (Pre-DNA) as the multi-species (M.S.) set from [66], arthropods from [3], or BS-1M. We compare models both with and without fine-tuning (FT) for each encoder.

| DNA enc. | Image enc. | Data sources | | | Species-level acc (%) | | |
|-------------|------------|--------------|--------|--------|-----------------------|-------------|-------------|
| | | Pre-DNA | FT-DNA | FT-Img | Seen | Unseen | H.M. |
| CNN encoder | RN-101 | - | INSECT | - | 38.3 | 20.8 | 27.0 |
| DNABERT-2 | RN-101 | M.S. | - | - | 36.2 | 10.4 | 16.2 |
| DNABERT-2 | RN-101 | M.S. | INSECT | - | 30.8 | 8.6 | 13.4 |
| BarcodeBERT | RN-101 | Arthro | - | - | 38.4 | 16.5 | 23.1 |
| BarcodeBERT | RN-101 | Arthro | INSECT | - | 37.3 | 20.8 | 26.7 |
| BarcodeBERT | ViT-B | Arthro | INSECT | - | 42.4 | 23.5 | 30.2 |
| BarcodeBERT | BS-CLIP-I | Arthro | INSECT | - | 42.4 | 22.4 | 29.3 |
| BarcodeBERT | BS-CLIP-I | Arthro | INSECT | INSECT | 46.9 | 22.9 | 30.7 |
| CNN encoder | BS-CLIP-I | - | INSECT | - | 44.3 | 21.0 | 28.5 |
| BarcodeBERT | BS-CLIP-I | Arthro | INSECT | INSECT | 46.9 | 22.9 | 30.7 |
| BS-CLIP-D | RN-101 | BS-1M | - | - | 36.7 | 22.4 | 27.8 |
| BS-CLIP-D | BS-CLIP-I | BS-1M | - | - | 51.3 | 22.6 | 31.4 |
| BS-CLIP-D | RN-101 | BS-1M | INSECT | - | 36.4 | 27.8 | 31.5 |
| BS-CLIP-D | BS-CLIP-I | BS-1M | INSECT | INSECT | 56.2 | 28.8 | 38.1 |

the highest performance after fine-tuning of 56.2% seen accuracy and 28.8% unseen accuracy. Thus, our model demonstrates the benefits of learning a shared embedding space relating image and DNA data, both in performance and the flexibility of applying to downstream tasks.

6. Conclusion

We introduce BIOSCAN-CLIP, an approach for integrating biological images with DNA barcodes and taxonomic labels to enhance taxonomic classification by using contrastive learning to align embeddings in a shared latent space. Due to their low-cost and ease of acquisition, images are the most practical modality for fostering inclusive participation in global biodiversity tracking efforts. We show the BIOSCAN-CLIP embedding space can be applied to fine-grained retrieval tasks for seen and unseen species, and leveraged flexibly for downstream tasks such as zero-shot learning. Underrepresented and unseen species pose the greatest challenge for our model, presenting an opportunity for future work.

Acknowledgement

We acknowledge the support of the Government of Canada’s New Frontiers in Research Fund (NFRF) [NFRFT-2020-00073]. AXC and GWT are also supported by Canada CIFAR AI Chair grants. JBH is supported by the Pioneer Centre for AI (DNRF grant number P1).

This research was enabled in part by support provided by the Digital Research Alliance of Canada (alliancecan.ca).

References

- [1] Hassan Akbari, Liangzhe Yuan, Rui Qian, Wei-Hong Chuang, Shih-Fu Chang, Yin Cui, and Boqing Gong. VATT: Transformers for multimodal self-supervised learning from raw video, audio and text. In *Advances in Neural Information Processing Systems*, pages 24206–24221. Curran Associates, Inc., 2021. 2
- [2] Jean-Baptiste Alayrac, Adria Recasens, Rosalia Schneider, Relja Arandjelović, Jason Ramapuram, Jeffrey De Fauw, Lucas Smaira, Sander Dieleman, and Andrew Zisserman. Self-supervised multimodal versatile networks. In *Advances in Neural Information Processing Systems*, pages 25–37. Curran Associates, Inc., 2020. 2
- [3] Pablo Millan Arias, Niousha Sadjadi, Monireh Safari, ZeMing Gong, Austin T. Wang, Scott C. Lowe, Joakim Bruslund Haurum, Iuliia Zarubiieva, Dirk Steinke, Lila Kari, Angel X. Chang, and Graham W. Taylor. BarcodeBERT: Transformers for biodiversity analysis. *arXiv preprint arXiv:2311.02401*, 2023. 1, 2, 3, 4, 8
- [4] Žiga Avsec, Vikram Agarwal, Daniel Visentin, Joseph R Leddam, Agnieszka Grabska-Barwinska, Kyle R Taylor, Yannis Assael, John Jumper, Pushmeet Kohli, and David R Kelley. Effective gene expression prediction from sequence by integrating long-range interactions. *Nature methods*, 18(10):1196–1203, 2021. 2
- [5] Sarkhan Badirli, Zeynep Akata, George Mohler, Christine Picard, and Mehmet M Dundar. Fine-grained zero-shot learning with DNA as side information. In *Advances in Neural Information Processing Systems*, pages 19352–19362. Curran Associates, Inc., 2021. 1, 2, 3, 5, 6, 7, 8
- [6] Sarkhan Badirli, Christine Johanna Picard, George Mohler, Frannie Richert, Zeynep Akata, and Murat Dundar. Classifying the unknown: Insect identification with deep hierarchical Bayesian learning. *Methods in Ecology and Evolution*, 14(6):1515–1530, 2023. 2, 3
- [7] Thomas Berg, Jiongxin Liu, Seung Woo Lee, Michelle L Alexander, David W Jacobs, and Peter N Belhumeur. Birdsnap: Large-scale fine-grained visual categorization of birds. In *2014 IEEE Conference on Computer Vision and Pattern Recognition*, pages 2019–2026, 2014. 2
- [8] Samuel Cahyawijaya, Tiezheng Yu, Zihan Liu, Xiaopu Zhou, Tze Wing Tiffany Mak, Yuk Yu Nancy Ip, and Pascale Fung. SNP2Vec: Scalable self-supervised pre-training for genome-wide association study. In *Proceedings of the 21st Workshop on Biomedical Language Processing*, pages 140–154, Dublin, Ireland, 2022. Association for Computational Linguistics. 1, 2
- [9] Mehdi Cherti, Romain Beaumont, Ross Wightman, Mitchell Wortsman, Gabriel Ilharco, Cade Gordon, Christoph Schuhmann, Ludwig Schmidt, and Jenia Jitsev. Reproducible scaling laws for contrastive language-image learning. In *Proceedings of the IEEE/CVF Conference on Computer Vision and Pattern Recognition*, pages 2818–2829, 2023. 2
- [10] Patrick John Chia, Giuseppe Attanasio, Federico Bianchi, Silvia Terragni, Ana Rita Magalhães, Diogo Goncalves, Ciro Greco, and Jacopo Tagliabue. Contrastive language and vision learning of general fashion concepts. *Scientific Reports*, 12(1):18958, 2022. 2
- [11] Sylvain Christin, Éric Hervet, and Nicolas Lecomte. Applications for deep learning in ecology. *Methods in Ecology and Evolution*, 10(10):1632–1644, 2019. 1
- [12] Elijah Cole, Xuan Yang, Kimberly Wilber, Oisín Mac Aodha, and Serge Belongie. When does contrastive visual representation learning work? In *Proceedings of the IEEE/CVF Conference on Computer Vision and Pattern Recognition*, pages 14755–14764, 2022. 2
- [13] Hugo Dalla-Torre, Liam Gonzalez, Javier Mendoza-Revilla, Nicolas Lopez Carranza, Adam Henryk Grzywaczewski, Francesco Oteri, Christian Dallago, Evan Trop, Bernardo P de Almeida, Hassan Sirelkhatim, et al. The nucleotide transformer: Building and evaluating robust foundation models for human genomics. *bioRxiv*, pages 2023–01, 2023. 2
- [14] Jacob Devlin, Ming-Wei Chang, Kenton Lee, and Kristina Toutanova. BERT: Pre-training of deep bidirectional transformers for language understanding. In *Proceedings of the 2019 Conference of the North American Chapter of the Association for Computational Linguistics: Human Language Technologies, Volume 1 (Long and Short Papers)*, pages 4171–4186, Minneapolis, Minnesota, 2019. Association for Computational Linguistics. 2
- [15] Alexey Dosovitskiy, Lucas Beyer, Alexander Kolesnikov, Dirk Weissenborn, Xiaohua Zhai, Thomas Unterthiner, Mostafa Dehghani, Matthias Minderer, Georg Heigold, Sylvain Gelly, Jakob Uszkoreit, and Neil Houlsby. An image is worth 16x16 words: Transformers for image recognition at scale. In *International Conference on Learning Representations*, 2021. 3, 8
- [16] Andreas Fürst, Elisabeth Rumetshofer, Johannes Lehner, Viet T. Tran, Fei Tang, Hubert Ramsauer, David Kreil, Michael Kopp, Günter Klambauer, Angela Bitto, and Sepp Hochreiter. CLOOB: Modern hopfield networks with InfoLOOB outperform CLIP. In *Advances in Neural Information Processing Systems*, pages 20450–20468. Curran Associates, Inc., 2022. 2
- [17] Camille Garcin, Alexis Joly, Pierre Bonnet, Antoine Afouard, Jean-Christophe Lombardo, Mathias Chouet, Maximilien Servajean, Titouan Lorieul, and Joseph Salmon. PI@ntNet-300K: a plant image dataset with high label ambiguity and a long-tailed distribution. In *Proceedings of the Neural Information Processing Systems Track on Datasets and Benchmarks*. Curran Associates, Inc., 2021. 1
- [18] Zahra Gharraee, ZeMing Gong, Nicholas Pellegrino, Iuliia Zarubiieva, Joakim Bruslund Haurum, Scott Lowe, Jaclyn McKeown, Chris Ho, Joschka McLeod, Yi-Yun Wei, Jireh Agda, Sujeevan Ratnasingham, Dirk Steinke, Angel Chang,

- Graham W Taylor, and Paul Fieguth. A step towards world-wide biodiversity assessment: The BIOSCAN-1M insect dataset. In *Advances in Neural Information Processing Systems*, pages 43593–43619. Curran Associates, Inc., 2024. [4](#), [5](#), [12](#)
- [19] Rohit Girdhar, Alaaeldin El-Nouby, Zhuang Liu, Mannat Singh, Kalyan Vasudev Alwala, Armand Joulin, and Ishan Misra. ImageBind: One embedding space to bind them all. In *Proceedings of the IEEE/CVF Conference on Computer Vision and Pattern Recognition (CVPR)*, pages 15180–15190, 2023. [2](#)
- [20] Shashank Goel, Hritik Bansal, Sumit Bhatia, Ryan Rossi, Vishwa Vinay, and Aditya Grover. CyCLIP: Cyclic contrastive language-image pretraining. In *Advances in Neural Information Processing Systems*, pages 6704–6719. Curran Associates, Inc., 2022. [2](#)
- [21] Yu Gu, Robert Tinn, Hao Cheng, Michael Lucas, Naoto Usuyama, Xiaodong Liu, Tristan Naumann, Jianfeng Gao, and Hoifung Poon. Domain-specific language model pre-training for biomedical natural language processing. *ACM Trans. Comput. Healthcare*, 3(1):1–23, 2021. [2](#)
- [22] Xiangteng He and Yuxin Peng. Fine-grained image classification via combining vision and language. In *Proceedings of the IEEE Conference on Computer Vision and Pattern Recognition*, pages 5994–6002, 2017. [2](#)
- [23] Paul D. N. Hebert, Alina Cywinska, Shelley L. Ball, and Jeremy R. deWaard. Biological identifications through DNA barcodes. *Proceedings of the Royal Society of London. Series B: Biological Sciences*, 270(1512):313–321, 2003. [1](#)
- [24] Edward J Hu, Yelong Shen, Phillip Wallis, Zeyuan Allen-Zhu, Yuanzhi Li, Shean Wang, Lu Wang, and Weizhu Chen. LoRA: Low-rank adaptation of large language models. In *International Conference on Learning Representations*, 2022. [3](#)
- [25] Wisdom Ikezogwo, Saygin Seyfioglu, Fatemeh Ghezloo, Dylan Geva, Fatwir Sheikh Mohammed, Pavan Kumar Anand, Ranjay Krishna, and Linda Shapiro. Quilt-1M: One million image-text pairs for histopathology. In *Advances in Neural Information Processing Systems*, pages 37995–38017. Curran Associates, Inc., 2023. [2](#)
- [26] Yanrong Ji, Zhihan Zhou, Han Liu, and Ramana V Davuluri. DNABERT: pre-trained bidirectional encoder representations from transformers model for DNA-language in genome. *Bioinformatics*, 37(15):2112–2120, 2021. [1](#), [2](#)
- [27] Chao Jia, Yinfei Yang, Ye Xia, Yi-Ting Chen, Zarana Parekh, Hieu Pham, Quoc Le, Yun-Hsuan Sung, Zhen Li, and Tom Duerig. Scaling up visual and vision-language representation learning with noisy text supervision. In *Proceedings of the 38th International Conference on Machine Learning*, pages 4904–4916. PMLR, 2021. [2](#)
- [28] Diederik Kingma and Jimmy Ba. Adam: A method for stochastic optimization. In *International Conference on Learning Representations (ICLR)*, San Diego, CA, USA, 2015. [5](#)
- [29] Nguyen Quoc Khanh Le, Quang-Thai Ho, Van-Nui Nguyen, and Jung-Su Chang. BERT-Promoter: An improved sequence-based predictor of dna promoter using bert pre-trained model and shap feature selection. *Computational Biology and Chemistry*, 99:107732, 2022. [2](#)
- [30] Dohoon Lee, Jeewon Yang, and Sun Kim. Learning the histone codes with large genomic windows and three-dimensional chromatin interactions using transformer. *Nature Communications*, 13(1):6678, 2022. [2](#)
- [31] Junnan Li, Dongxu Li, Caiming Xiong, and Steven Hoi. BLIP: Bootstrapping language-image pre-training for unified vision-language understanding and generation. In *Proceedings of the International Conference on Machine Learning*, pages 12888–12900. PMLR, 2022. [2](#)
- [32] Junnan Li, Dongxu Li, Silvio Savarese, and Steven Hoi. BLIP-2: Bootstrapping language-image pre-training with frozen image encoders and large language models. *arXiv preprint arXiv:2301.12597*, 2023.
- [33] Liunian Harold Li, Pengchuan Zhang, Haotian Zhang, Jianwei Yang, Chunyuan Li, Yiwu Zhong, Lijuan Wang, Lu Yuan, Lei Zhang, Jenq-Neng Hwang, et al. Grounded language-image pre-training. In *Proceedings of the IEEE/CVF Conference on Computer Vision and Pattern Recognition*, pages 10965–10975, 2022. [2](#)
- [34] Yangguang Li, Feng Liang, Lichen Zhao, Yufeng Cui, Wanli Ouyang, Jing Shao, Fengwei Yu, and Junjie Yan. Supervision exists everywhere: A data efficient contrastive language-image pre-training paradigm. In *10th International Conference on Learning Representations*, 2022. [2](#)
- [35] Zhongxiao Li, Elva Gao, Juexiao Zhou, Wenkai Han, Xiaopeng Xu, and Xin Gao. Applications of deep learning in understanding gene regulation. *Cell Reports Methods*, 3(1):100384, 2023. [2](#)
- [36] Qiaoxing Liang, Paul W Bible, Yu Liu, Bin Zou, and Lai Wei. DeepMicrobes: taxonomic classification for metagenomics with deep learning. *NAR Genomics and Bioinformatics*, 2(1):lqaa009, 2020. [2](#)
- [37] Ming Y Lu, Bowen Chen, Drew FK Williamson, Richard J Chen, Ivy Liang, Tong Ding, Guillaume Jaume, Igor Odintsov, Andrew Zhang, Long Phi Le, et al. Towards a visual-language foundation model for computational pathology. *arXiv preprint arXiv:2307.12914*, 2023. [2](#)
- [38] D. H. Lunt, D.-X. Zhang, J. M. Szymura, and O. M. Hewlitt. The insect cytochrome oxidase I gene: evolutionary patterns and conserved primers for phylogenetic studies. *Insect Molecular Biology*, 5(3):153–165, 1996. [1](#)
- [39] Oisín Mac Aodha, Elijah Cole, and Pietro Perona. Presence-only geographical priors for fine-grained image classification. In *Proceedings of the IEEE/CVF International Conference on Computer Vision (ICCV)*, pages 9596–9606, 2019. [2](#)
- [40] Chloé Martineau, Donatello Conte, Romain Raveaux, Ingrid Arnault, Damien Munier, and Gilles Venturini. A survey on image-based insect classification. *Pattern Recognition*, 65:273–284, 2017. [1](#)
- [41] Leland McInnes, John Healy, and James Melville. UMAP: Uniform manifold approximation and projection for dimension reduction. *arXiv preprint arXiv:1802.03426*, 2018. [14](#)
- [42] Florian Mock, Fleming Kretschmer, Anton Kriese, Sebastian Böcker, and Manja Marz. Taxonomic classification of DNA

- sequences beyond sequence similarity using deep neural networks. *Proceedings of the National Academy of Sciences*, 119(35):e2122636119, 2022. 1, 2
- [43] Eric Nguyen, Michael Poli, Marjan Faizi, Armin Thomas, Michael Wornow, Callum Birch-Sykes, Stefano Massaroli, Aman Patel, Clayton Rabideau, Yoshua Bengio, Stefano Ermon, Christopher Ré, and Stephen Baccus. HyenaDNA: Long-range genomic sequence modeling at single nucleotide resolution. In *Advances in Neural Information Processing Systems*, pages 43177–43201. Curran Associates, Inc., 2023. 2
- [44] Hoang-Quan Nguyen, Thanh-Dat Truong, Xuan Bac Nguyen, Ashley Dowling, Xin Li, and Khoa Luu. Insect-Foundation: A foundation model and large-scale 1M dataset for visual insect understanding. *arXiv preprint arXiv:2311.15206*, 2023. 2
- [45] Andrew Owens and Alexei A. Efros. Audio-visual scene analysis with self-supervised multisensory features. In *Proceedings of the European Conference on Computer Vision (ECCV)*, 2018. 2
- [46] Gerald Piosenka. Birds 525 species - image classification, 2023. 2
- [47] Alec Radford, Jong Wook Kim, Chris Hallacy, Aditya Ramesh, Gabriel Goh, Sandhini Agarwal, Girish Sastry, Amanda Askell, Pamela Mishkin, Jack Clark, Gretchen Krueger, and Ilya Sutskever. Learning transferable visual models from natural language supervision. In *Proceedings of the International Conference on Machine Learning*, pages 8748–8763. PMLR, 2021. 1, 2, 3
- [48] Marko Ristin, Juergen Gall, Matthieu Guillaumin, and Luc Van Gool. From categories to subcategories: large-scale image classification with partial class label refinement. In *Proceedings of the IEEE Conference on Computer Vision and Pattern Recognition (CVPR)*, pages 231–239, 2015. 2
- [49] Yue Ruan, Han-Hung Lee, Yiming Zhang, Ke Zhang, and Angel X Chang. TriCoLo: Trimodal contrastive loss for text to shape retrieval. In *Proceedings of the IEEE/CVF Winter Conference on Applications of Computer Vision*, pages 5815–5825, 2024. 2, 3
- [50] Kihyuk Sohn. Improved deep metric learning with multi-class n-pair loss objective. In *Advances in Neural Information Processing Systems*. Curran Associates, Inc., 2016. 3
- [51] Kaitao Song, Xiu-Shen Wei, Xiangbo Shu, Ren-Jie Song, and Jianfeng Lu. Bi-modal progressive mask attention for fine-grained recognition. *IEEE Transactions on Image Processing*, 29:7006–7018, 2020. 2
- [52] Samuel Stevens, Jiaman Wu, Matthew J Thompson, Elizabeth G Campolongo, Chan Hee Song, David Edward Caryl, Li Dong, Wasila M Dahdul, Charles Stewart, Tanya Berger-Wolf, Wei-Lun Chao, and Yu Su. BioCLIP: A vision foundation model for the tree of life. *arXiv preprint arXiv:2311.18803*, 2023. 1, 2, 4, 7
- [53] Nigel E Stork. How many species of insects and other terrestrial arthropods are there on Earth? *Annual review of entomology*, 63(1):31–45, 2018. PMID: 28938083. 4
- [54] Fariborz Taherkhani, Hadi Kazemi, Ali Dabouei, Jeremy Dawson, and Nasser M. Nasrabadi. A weakly supervised fine label classifier enhanced by coarse supervision. In *Proceedings of the IEEE/CVF International Conference on Computer Vision (ICCV)*, pages 6459–6468, 2019. 2
- [55] Christina V. Theodoris, Ling Xiao, Anant Chopra, Mark D. Chaffin, Zeina R. Al Sayed, Matthew C. Hill, Helene Mantiño, Elizabeth M. Brydon, Zexian Zeng, X. Shirley Liu, and Patrick T. Ellinor. Transfer learning enables predictions in network biology. *Nature*, 618(7965):616–624, 2023. 2
- [56] Hugo Touvron, Alexandre Sablayrolles, Matthijs Douze, Matthieu Cord, and Hervé Jégou. Graft: Learning fine-grained image representations with coarse labels. In *Proceedings of the IEEE/CVF international conference on computer vision*, pages 874–884, 2021. 2
- [57] Iulia Turc, Ming-Wei Chang, Kenton Lee, and Kristina Toutanova. Well-read students learn better: On the importance of pre-training compact models. *arXiv preprint arXiv:1908.08962*, 2019. 3
- [58] Grant Van Horn, Oisín Mac Aodha, Yang Song, Yin Cui, Chen Sun, Alex Shepard, Hartwig Adam, Pietro Perona, and Serge Belongie. The iNaturalist species classification and detection dataset. In *Proceedings of the IEEE conference on computer vision and pattern recognition*, pages 8769–8778, 2018. 1, 2
- [59] Sagar Vaze, Kai Han, Andrea Vedaldi, and Andrew Zisserman. Open-set recognition: a good closed-set classifier is all you need? In *10th International Conference on Learning Representations*, 2022. 6
- [60] Xiu-Shen Wei, Yi-Zhe Song, Oisín Mac Aodha, Jianxin Wu, Yuxin Peng, Jinhui Tang, Jian Yang, and Serge Belongie. Fine-grained image analysis with deep learning: A survey. *IEEE Transactions on Pattern Analysis and Machine Intelligence*, 44(12):8927–8948, 2022. 1, 2
- [61] Tete Xiao, Xiaolong Wang, Alexei A Efros, and Trevor Darrell. What should not be contrastive in contrastive learning. In *International Conference on Learning Representations*, 2021. 2
- [62] Xiaohua Zhai, Basil Mustafa, Alexander Kolesnikov, and Lucas Beyer. Sigmoid loss for language image pre-training. *arXiv preprint arXiv:2303.15343*, 2023. 2
- [63] Hua Zhang, Xiaochun Cao, and Rui Wang. Audio visual attribute discovery for fine-grained object recognition. In *Proceedings of the AAAI Conference on Artificial Intelligence*, 2018. 2
- [64] Sheng Zhang, Yanbo Xu, Naoto Usuyama, Hanwen Xu, Jaspreet Bagga, Robert Tinn, Sam Preston, Rajesh Rao, Mu Wei, Naveen Valluri, Cliff Wong, Andrea Tupini, Yu Wang, Matt Mazzola, Swadheen Shukla, Lars Liden, Jianfeng Gao, Matthew P. Lungren, Tristan Naumann, Sheng Wang, and Hoifung Poon. BiomedCLIP: a multimodal biomedical foundation model pretrained from fifteen million scientific image-text pairs. *arXiv preprint arXiv:2303.00915*, 2024. 2
- [65] Yuhao Zhang, Hang Jiang, Yasuhide Miura, Christopher D. Manning, and Curtis P. Langlotz. Contrastive learning of medical visual representations from paired images and text. In *Proceedings of the 7th Machine Learning for Healthcare Conference*, pages 2–25. PMLR, 2022. 3
- [66] Zhihan Zhou, Yanrong Ji, Weijian Li, Pratik Dutta, Ramana V Davuluri, and Han Liu. DNABERT-2: Effi-

cient foundation model and benchmark for multi-species genomes. In *International Conference on Learning Representations*, 2024. 1, 2, 8

- [67] Zhihan Zhou, Weimin Wu, Harrison Ho, Jiayi Wang, Lizhen Shi, Ramana V Davuluri, Zhong Wang, and Han Liu. DNABERT-S: Learning species-aware DNA embedding with genome foundation models. *arXiv preprint arXiv:2402.08777*, 2024. 2

Appendices

We provide additional details on how we obtain our data split (Appendix A) and additional experiments (Appendix B) comparing against baselines, evaluating on the test set, and applying DNA features as queries for inference.

A. Additional data details

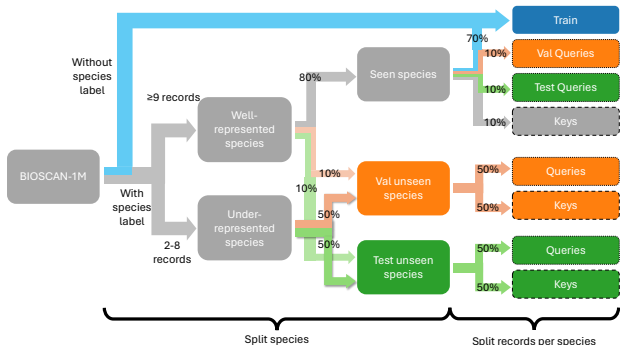


Figure 6. *Data partitioning strategy*. We first partition species among the splits based on the presence of a species label and the number of records per species, and then each species is designated as seen or unseen. Records from each species are then partitioned among train (blue), validation (orange), and test (green). For the validation and test sets, some records are used as *queries*, and the rest are used as *keys* for the reference database for retrieval.

We use a multi-stage process to establish our split of BIOSCAN-1M [18] for our experiments (see Figure 6). Firstly, we separate records with and without species labels. Any record without a species label is allocated for pretraining, as we cannot easily use them during evaluation. Of the remaining records with labelled species, we partition species based on their number of samples. Species with at least 9 records are allocated 80/20 to *seen* and *unseen*, with unseen records split evenly between validation and test. Species with 2 to 8 records are used only as unseen species, with a partition of 50/50 between validation and test. This allows us to simulate real-world scenarios, in which most of our unseen species are represented only by a few records, ensuring a realistic distribution of species sets. Species with only one record are excluded, as we need at least one record each to act the query and the key, respectively.

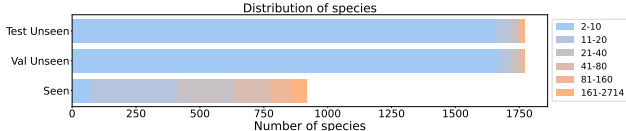


Figure 7. Distribution of species among the seen, validation unseen, and test unseen splits. Since all of the train, validation, and test seen splits share the same species, we represent them collectively. The coloured blocks within each bar represent the numbers of records available for that species, demonstrating that most of the species in the unseen splits have few records.

Finally, we allocate the records within each species into designated partitions. For the seen species, we subdivide the records at a 70/10/10/10 ratio into train/val/test/key, where the keys for the seen species are shared across all splits. The unseen species for each of validation and test are split evenly between queries and keys. The allocation of queries and keys ensures that we have clearly designated samples as inputs and target references for inference. We note that some samples in our data may have the exact same barcode even though the image may differ. Figure 7 shows the number of species in our dataset and the distribution of records for each species. Note that we have a few species with a many records, and many species with just a few records.

B. Additional Experiments

In this section, we include additional experimental results and visualizations. We report additional results on querying with images to compare against additional baselines (Appendix B.1) and assess the model’s performance using DNA as queries (Appendix B.2). We also visualize the aligned embedding space (Appendix B.3) to demonstrate the model’s capability in integrating and representing diverse biological data. Finally, we report performance over a range of batch sizes (Appendix B.4).

B.1. Additional results for querying with images

Complete results on validation and test set. To complement Table 1 in our main paper and provide more comprehensive results, we have introduced Table 7 and Table 8. These new tables show the Top-1 accuracy at various taxonomic levels for BIOSCAN-CLIP, following contrastive pretraining with different combinations of modalities. Specifically, they detail the performance when using **image features as queries** and features from images, DNA barcodes, and the average of image and DNA barcode features as keys. Overall, we see that on both the test and validation sets, using the complete model (with image, DNA, and text aligned) gives the best overall results. We also note that querying image-to-image embedding is the most effective on unseen species.

Table 7. Top-1 accuracy (%) on the *validation* set for different combinations of aligned embeddings (image, DNA, text) during contrastive training, using *image* embedding to match against different embeddings for retrieval (Image, DNA, average of Image and DNA). The best results across trained models are shown in **bold**, and the best embedding key for the Image+DNA+Text model is indicated in **blue**.

| Taxon | Alignment | | | Micro top-1 accuracy | | | | | | | | | Macro top-1 accuracy | | | | | | | | |
|---------|-----------|----------|----------|----------------------|-------------|-------------|-------------|-------------|-------------|-------------|-------------|-------------|----------------------|-------------|-------------|-------------|-------------|-------------|-------------|-------------|-------------|
| | | | | Seen | | | Unseen | | | H.M. | | | Seen | | | Unseen | | | H.M. | | |
| | Img | DNA | Txt | Img | DNA | Avg | Img | DNA | Avg | Img | DNA | Avg | Img | DNA | Avg | Img | DNA | Avg | Img | DNA | Avg |
| Order | <i>x</i> | <i>x</i> | <i>x</i> | 95.4 | 41.3 | 95.7 | 95.2 | 38.3 | 95.1 | 95.3 | 39.8 | 95.4 | 60.7 | 12.8 | 60.6 | 51.8 | 8.7 | 54.0 | 55.9 | 10.4 | 57.1 |
| | ✓ | <i>x</i> | ✓ | 99.3 | – | – | 99.1 | – | – | 99.2 | – | – | 98.2 | – | – | 90.9 | – | – | 94.4 | – | – |
| | ✓ | ✓ | <i>x</i> | 99.2 | 98.5 | 99.3 | 99.0 | 97.6 | 98.6 | 99.1 | 98.0 | 99.0 | 98.0 | 87.4 | 88.5 | 78.7 | 52.6 | 71.7 | 87.3 | 65.7 | 79.2 |
| | ✓ | ✓ | ✓ | 99.3 | 98.7 | 99.3 | 99.2 | 97.6 | 98.7 | 99.3 | 98.2 | 99.0 | 98.0 | 97.2 | 98.3 | 84.9 | 58.8 | 76.7 | 91.0 | 73.2 | 86.2 |
| Family | <i>x</i> | <i>x</i> | <i>x</i> | 69.5 | 3.3 | 68.8 | 73.7 | 4.8 | 73.2 | 71.6 | 3.9 | 70.9 | 42.6 | 1.1 | 42.4 | 35.7 | 0.7 | 35.4 | 38.9 | 0.8 | 38.6 |
| | ✓ | <i>x</i> | ✓ | 89.1 | – | – | 88.7 | – | – | 88.9 | – | – | 74.9 | – | – | 64.2 | – | – | 69.2 | – | – |
| | ✓ | ✓ | <i>x</i> | 87.9 | 80.4 | 89.1 | 87.9 | 74.0 | 74.0 | 87.9 | 77.1 | 86.0 | 73.7 | 50.4 | 74.9 | 62.4 | 28.3 | 48.9 | 67.6 | 36.2 | 59.2 |
| | ✓ | ✓ | ✓ | 90.5 | 84.6 | 91.7 | 89.1 | 79.0 | 86.2 | 89.8 | 81.7 | 88.9 | 80.1 | 56.3 | 78.0 | 65.6 | 35.2 | 58.0 | 72.2 | 43.3 | 66.5 |
| Genus | <i>x</i> | <i>x</i> | <i>x</i> | 45.1 | 0.9 | 44.7 | 52.7 | 3.1 | 52.6 | 48.6 | 1.5 | 48.3 | 24.6 | 0.1 | 24.3 | 19.7 | 0.1 | 20.0 | 21.9 | 0.1 | 22.0 |
| | ✓ | <i>x</i> | ✓ | 69.7 | – | – | 70.1 | – | – | 69.9 | – | – | 49.3 | – | – | 40.3 | – | – | 44.4 | – | – |
| | ✓ | ✓ | <i>x</i> | 71.3 | 52.2 | 73.6 | 71.7 | 37.0 | 37.0 | 71.5 | 43.3 | 65.7 | 52.4 | 24.7 | 52.1 | 42.0 | 7.9 | 27.7 | 46.6 | 12.0 | 36.2 |
| | ✓ | ✓ | ✓ | 74.8 | 58.5 | 76.9 | 73.4 | 43.5 | 64.0 | 74.1 | 49.9 | 69.9 | 57.0 | 30.1 | 56.2 | 46.0 | 11.7 | 35.0 | 50.9 | 16.8 | 43.2 |
| Species | <i>x</i> | <i>x</i> | <i>x</i> | 29.6 | 0.0 | 29.4 | 41.1 | 2.0 | 41.1 | 34.3 | 0.0 | 34.3 | 14.1 | 0.0 | 14.1 | 10.5 | 0.0 | 10.6 | 12.1 | 0.0 | 12.1 |
| | ✓ | <i>x</i> | ✓ | 53.0 | – | – | 57.6 | – | – | 55.2 | – | – | 32.7 | – | – | 24.2 | – | – | 27.8 | – | – |
| | ✓ | ✓ | <i>x</i> | 56.7 | 37.5 | 60.8 | 60.7 | 17.1 | 46.9 | 58.7 | 23.5 | 52.9 | 36.3 | 15.6 | 37.1 | 26.3 | 2.5 | 15.3 | 30.5 | 4.3 | 21.7 |
| | ✓ | ✓ | ✓ | 60.4 | 42.0 | 63.7 | 62.5 | 30.1 | 50.4 | 61.4 | 35.1 | 56.2 | 40.4 | 17.4 | 40.9 | 30.4 | 3.9 | 20.3 | 34.7 | 6.4 | 27.2 |

Table 8. Top-1 accuracy (%) on the *test* set for different combinations of aligned embeddings (image, DNA, text) during contrastive training, using image embedding to match against different embeddings for retrieval (Image, DNA, average of Image and DNA). The best results across trained models are shown in **bold**, and the best embedding key for the Image+DNA+Text model is indicated in **blue**. We observe similar trends as for the validation set, with the Image+DNA+Text model performing the best and the best performance largely achieved when using images as keys.

| Taxon | Alignment | | | Micro top-1 accuracy | | | | | | | | | Macro top-1 accuracy | | | | | | | | |
|---------|-----------|----------|----------|----------------------|-------------|-------------|-------------|-------------|-------------|-------------|-------------|-------------|----------------------|-------------|-------------|-------------|-------------|-------------|-------------|-------------|-------------|
| | | | | Seen | | | Unseen | | | H.M. | | | Seen | | | Unseen | | | H.M. | | |
| | Img | DNA | Txt | Img | DNA | Avg | Img | DNA | Avg | Img | DNA | Avg | Img | DNA | Avg | Img | DNA | Avg | Img | DNA | Avg |
| Order | <i>x</i> | <i>x</i> | <i>x</i> | 95.0 | 55.0 | 94.6 | 95.6 | 48.2 | 95.2 | 95.3 | 51.4 | 94.9 | 72.0 | 10.0 | 71.3 | 71.2 | 8.0 | 63.0 | 71.6 | 8.9 | 66.9 |
| | ✓ | <i>x</i> | ✓ | 99.3 | – | – | 99.1 | – | – | 99.2 | – | – | 89.1 | – | – | 90.5 | – | – | 89.8 | – | – |
| | ✓ | ✓ | <i>x</i> | 99.2 | 98.5 | 99.2 | 99.0 | 97.7 | 98.8 | 99.1 | 98.1 | 99.0 | 78.3 | 87.2 | 88.6 | 83.4 | 73.8 | 86.7 | 80.8 | 79.9 | 87.7 |
| | ✓ | ✓ | ✓ | 99.3 | 98.7 | 99.4 | 99.1 | 97.7 | 99.0 | 99.2 | 98.2 | 99.2 | 99.0 | 86.9 | 89.2 | 93.3 | 71.8 | 82.3 | 96.0 | 78.6 | 85.6 |
| Family | <i>x</i> | <i>x</i> | <i>x</i> | 68.5 | 1.3 | 67.0 | 71.7 | 1.0 | 70.2 | 70.0 | 1.1 | 68.5 | 45.8 | 0.6 | 44.1 | 36.3 | 0.4 | 35.4 | 40.5 | 0.5 | 39.3 |
| | ✓ | <i>x</i> | ✓ | 89.6 | – | – | 87.0 | – | – | 88.3 | – | – | 76.6 | – | – | 60.9 | – | – | 67.9 | – | – |
| | ✓ | ✓ | <i>x</i> | 88.2 | 80.8 | 89.6 | 85.9 | 70.3 | 83.3 | 87.0 | 75.2 | 86.4 | 76.0 | 50.0 | 77.6 | 59.9 | 26.9 | 52.9 | 67.0 | 35.0 | 62.9 |
| | ✓ | ✓ | ✓ | 89.9 | 85.9 | 92.0 | 87.3 | 76.0 | 86.0 | 88.6 | 80.7 | 88.9 | 77.9 | 60.2 | 80.1 | 63.5 | 31.3 | 59.4 | 70.0 | 41.2 | 68.2 |
| Genus | <i>x</i> | <i>x</i> | <i>x</i> | 43.8 | 0.3 | 42.5 | 49.9 | 0.1 | 48.5 | 46.6 | 0.1 | 45.3 | 25.5 | 0.2 | 24.1 | 17.7 | 0.1 | 16.5 | 20.9 | 0.1 | 19.6 |
| | ✓ | <i>x</i> | ✓ | 70.1 | – | – | 66.6 | – | – | 68.3 | – | – | 50.6 | – | – | 35.2 | – | – | 41.5 | – | – |
| | ✓ | ✓ | <i>x</i> | 72.9 | 53.0 | 75.1 | 68.1 | 37.3 | 60.1 | 70.4 | 43.8 | 66.8 | 53.8 | 25.0 | 55.8 | 38.9 | 8.7 | 31.5 | 45.1 | 13.0 | 40.3 |
| | ✓ | ✓ | ✓ | 74.4 | 58.7 | 77.5 | 70.1 | 40.3 | 64.0 | 72.2 | 47.8 | 70.1 | 56.0 | 30.7 | 60.9 | 41.7 | 9.0 | 36.5 | 47.8 | 13.9 | 45.6 |
| Species | <i>x</i> | <i>x</i> | <i>x</i> | 29.3 | 0.2 | 27.8 | 35.8 | 0.0 | 34.9 | 32.2 | 0.0 | 30.9 | 15.1 | 0.1 | 14.5 | 9.4 | 0 | 8.6 | 11.6 | – | 10.8 |
| | ✓ | <i>x</i> | ✓ | 52.8 | – | – | 51.1 | – | – | 51.9 | – | – | 32.3 | – | – | 22.3 | – | – | 26.4 | – | – |
| | ✓ | ✓ | <i>x</i> | 58.0 | 37.2 | 61.7 | 53.1 | 16.9 | 42.6 | 55.5 | 23.3 | 50.4 | 37.2 | 14.3 | 38.2 | 24.6 | 2.3 | 18.9 | 29.6 | 4.0 | 25.3 |
| | ✓ | ✓ | ✓ | 59.7 | 42.3 | 63.9 | 56.2 | 20.1 | 46.1 | 57.9 | 27.2 | 53.8 | 38.7 | 17.1 | 42.4 | 27.9 | 2.3 | 22.9 | 32.4 | 4.0 | 29.7 |

B.2. Querying using DNA features

While our main focus was in the practical scenario where we have a new image query, we also report results here for querying with DNA barcodes, when they are available. We report results with DNA embedding as the query in **Table 9**. We note that DNA-to-DNA queries give considerably higher performance than querying with images. This is not unexpected as DNA is more disguising for species identification, and as we noted there may even be some DNA barcodes that are identical across samples. However, it is

typically more expensive to obtain samples with DNA versus images. We show examples of the top-5 matched samples using DNA-to-DNA retrieval in **Figure 8**. Even when querying and retrieving based on DNA, we observe photometric similarities between the corresponding insect images.

B.3. Embedding space visualization

To better understand the alignment of features in the embedding space, we visualize a mapping of the image and

Table 9. Top-1 accuracy (%) on the *validation* set for different combinations of aligned embeddings (image, DNA, text) during contrastive training, using *DNA* embeddings as queries to match against different embeddings for retrieval (Image, DNA, and average of Image and DNA). The best results across trained models are shown in **bold** and the best embedding key for the Image+DNA+Text model is indicated in **blue**. Direct querying with DNA-to-DNA gives the best performance, but DNA may not always be available for a new sample.

| Taxon | Alignment | | | Micro top-1 accuracy | | | | | | | | | Macro top-1 accuracy | | | | | | | | |
|---------|-----------|-----|-----|----------------------|--------------|--------------|-------------|--------------|--------------|-------------|--------------|--------------|----------------------|--------------|--------------|-------------|-------------|--------------|-------------|--------------|--------------|
| | | | | Seen | | | Unseen | | | H.M. | | | Seen | | | Unseen | | | H.M. | | |
| | Img | DNA | Txt | Img | DNA | Avg | Img | DNA | Avg | Img | DNA | Avg | Img | DNA | Avg | Img | DNA | Avg | Img | DNA | Avg |
| Order | x | x | x | 32.6 | 98.6 | 63.0 | 45.8 | 97.5 | 65.7 | 38.1 | 98.0 | 64.3 | 12.1 | 87.8 | 16.3 | 9.7 | 75.0 | 13.0 | 10.8 | 80.9 | 14.5 |
| | ✓ | ✓ | x | 99.7 | 99.9 | 99.9 | 98.2 | 99.9 | 99.8 | 98.9 | 100.0 | 99.9 | 79.4 | 100.0 | 99.9 | 57.7 | 99.9 | 99.1 | 66.8 | 99.9 | 99.5 |
| | ✓ | ✓ | ✓ | 100.0 | 100.0 | 100.0 | 99.3 | 100.0 | 100.0 | 99.6 | 100.0 | 100.0 | 79.8 | 100.0 | 100.0 | 70.4 | 99.9 | 100.0 | 74.8 | 100.0 | 100.0 |
| Family | x | x | x | 7.1 | 94.6 | 10.7 | 13.6 | 92.1 | 12.6 | 9.3 | 93.4 | 11.6 | 1.0 | 82.5 | 1.6 | 0.7 | 69.4 | 1.1 | 0.8 | 75.4 | 1.3 |
| | ✓ | ✓ | x | 86.6 | 97.8 | 96.1 | 80.4 | 95.6 | 90.3 | 83.3 | 96.7 | 93.1 | 53.9 | 90.4 | 80.1 | 32.8 | 81.3 | 60.5 | 40.76 | 85.6 | 68.9 |
| | ✓ | ✓ | ✓ | 91.2 | 99.5 | 99.1 | 83.8 | 98.2 | 96.1 | 87.4 | 98.8 | 97.6 | 62.0 | 96.6 | 94.6 | 39.0 | 90.8 | 79.7 | 47.9 | 93.6 | 86.5 |
| Genus | x | x | x | 1.0 | 91.6 | 4.7 | 0.5 | 87.2 | 0.7 | 0.6 | 89.3 | 1.2 | 0.2 | 78.9 | 0.4 | 0.1 | 64.3 | 0.2 | 0.2 | 70.8 | 0.3 |
| | ✓ | ✓ | x | 61.0 | 92.2 | 84.5 | 43.9 | 85.3 | 70.0 | 51.1 | 88.6 | 76.6 | 25.9 | 79.3 | 59.2 | 8.5 | 63.9 | 33.2 | 12.8 | 70.8 | 42.5 |
| | ✓ | ✓ | ✓ | 66.5 | 96.6 | 93.2 | 46.1 | 91.7 | 81.7 | 54.5 | 94.1 | 87.1 | 30.5 | 89.2 | 80.5 | 11.9 | 78.2 | 56.9 | 17.1 | 83.4 | 66.7 |
| Species | x | x | x | 0.0 | 88.5 | 0.4 | 0.0 | 83.4 | 0.0 | 0.0 | 85.9 | 0.0 | 0.0 | 73.9 | 0.1 | 0.0 | 59.0 | 0.0 | 0.0 | 65.6 | 0.0 |
| | ✓ | ✓ | x | 43.0 | 86.3 | 75.3 | 31.3 | 76.7 | 57.7 | 36.2 | 81.2 | 65.3 | 14.0 | 68.9 | 46.1 | 2.9 | 48.2 | 19.8 | 4.8 | 56.7 | 27.6 |
| | ✓ | ✓ | ✓ | 49.1 | 91.7 | 86.0 | 32.0 | 84.8 | 70.9 | 38.7 | 88.1 | 77.7 | 18.0 | 79.1 | 67.3 | 3.6 | 63.2 | 40.2 | 6.0 | 70.3 | 50.3 |

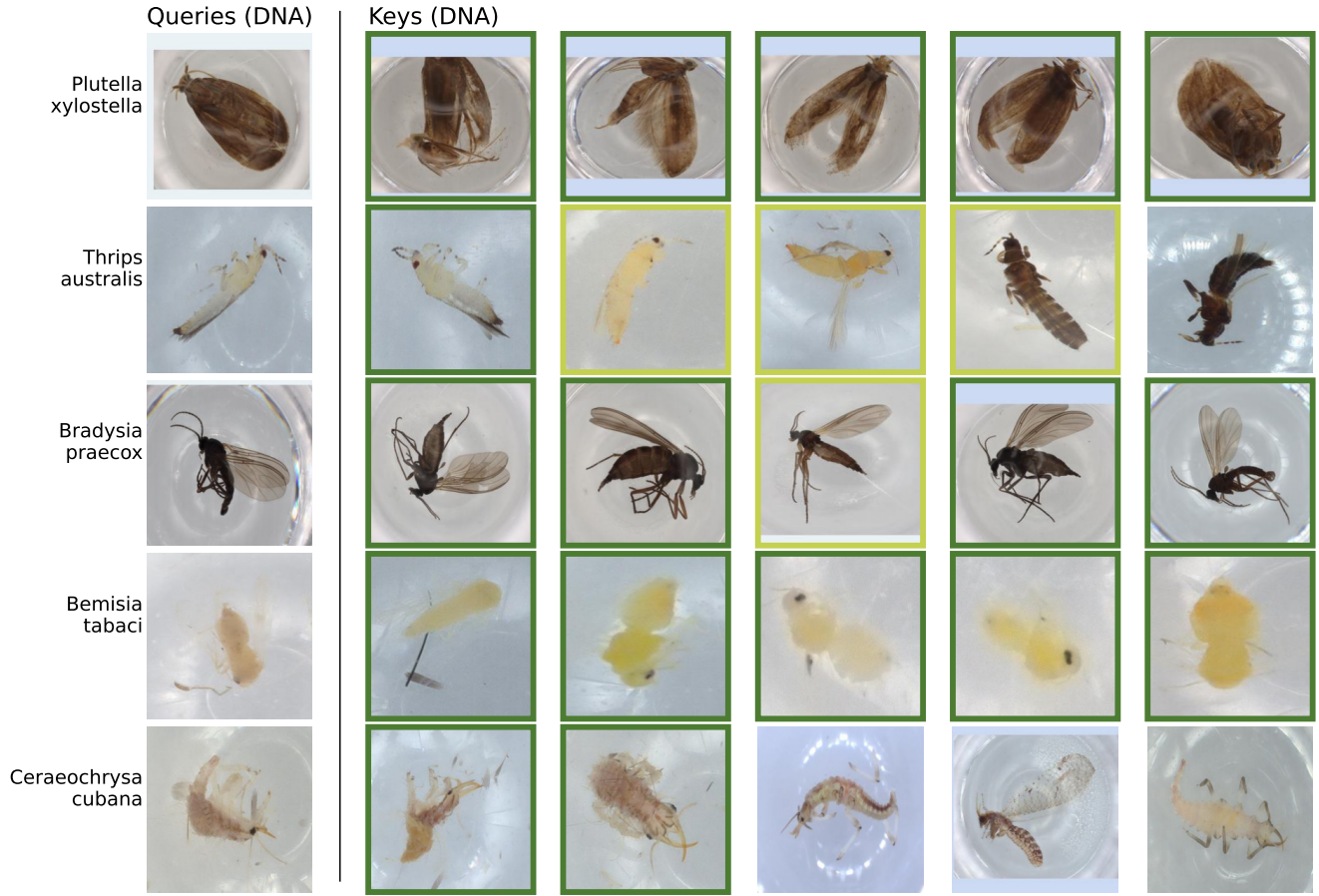


Figure 8. *Example DNA query-key pairs.* For five distinct DNA barcode queries, we show the top-5 nearest specimens from the validation-key dataset retrieved based on the cosine-distance between the DNA feature query and DNA feature keys. Surrounding boxes denote keys of the same species (dark green) or same genus (yellow) as the query specimen.

DNA embeddings in **Figure 9**. We use UMAP [41] with a cosine similarity metric applied to the seen validation set to

map the embeddings down to 2D space, and we mark points in the space based on their order classification. We observe

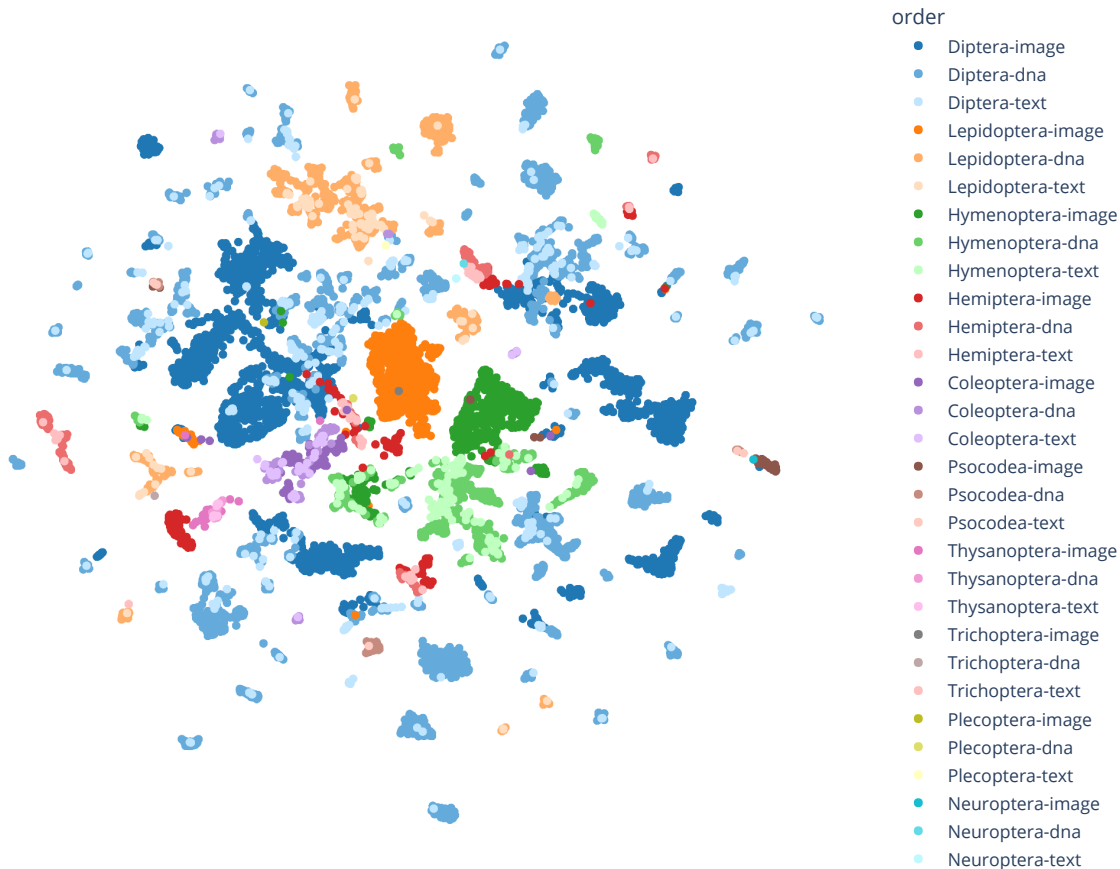


Figure 9. *Embedding visualization.* We visualize the embedding space of the seen validation set generated using UMAP on the image, DNA, and text embeddings, using a cosine similarity distance metric. Marker hue: order taxon. Marker lightness: data modality.

that, for some orders, there are numerous outlier clusters spread out in the space. However, overall the orders demonstrate some degree of clustering together, with image and DNA features close to one another within their respective clusters. Furthermore, we note the text embeddings tend to lie within the Image or (more often) DNA clusters, suggesting a good alignment between text and other modalities.

B.4. Batch size experiments

We conduct additional experiments and present in [Table 10](#) the impact of using different batch sizes on classification accuracy across various taxonomic levels. While the batch size typically does not have a major impact on performance when using supervised learning, the batch size has more impact on contrastive learning training paradigms since the number of negative pairs per iteration scales quadratically with the batch size.

Our results indicate that as the batch size increases, the classification accuracy improves. This improvement in accuracy becomes more pronounced as the taxonomic level decreases. Therefore, we believe that using larger

batch sizes can further enhance the classification accuracy of BIOSCAN-CLIP, especially on more fine-grained taxonomic levels.

Table 10. Top-1 accuracy on the validation set with models that are contrastive pretrained with different batch sizes with image queries. Training at larger batch sizes is helpful for improving accuracy at more fine-grained taxonomic levels such as genus and species.

| Taxon | Batch size | Micro top-1 accuracy | | | | | | | | | | | Macro top-1 accuracy | | | | | | | | | |
|---------|------------|----------------------|-----|-----|-------------|-------------|-------------|-------------|-------------|-------------|-------------|-------------|----------------------|-------------|-------------|-------------|-------------|-------------|-------------|-------------|-------------|-------------|
| | | Alignment | | | Seen | | | Unseen | | | H.M. | | | Seen | | | Unseen | | | H.M. | | |
| | | Img | DNA | Txt | Img | DNA | Avg | Img | DNA | Avg | Img | DNA | Avg | Img | DNA | Avg | Img | DNA | Avg | Img | DNA | Avg |
| Order | 200 | ✓ | ✓ | ✓ | 99.3 | 98.8 | 99.4 | 99.1 | 97.9 | 98.9 | 99.2 | 98.4 | 99.2 | 88.1 | 87.9 | 98.6 | 79.5 | 55.5 | 78.6 | 83.5 | 68.0 | 87.5 |
| | 400 | ✓ | ✓ | ✓ | 99.5 | 99.0 | 99.5 | 99.1 | 98.0 | 99.1 | 99.3 | 98.5 | 99.3 | 98.5 | 87.8 | 99.0 | 84.5 | 62.4 | 79.8 | 91.0 | 72.9 | 88.4 |
| | 600 | ✓ | ✓ | ✓ | 99.4 | 98.5 | 99.5 | 99.3 | 97.8 | 99.1 | 99.4 | 98.1 | 99.3 | 98.6 | 76.3 | 98.2 | 87.9 | 52.5 | 87.6 | 92.9 | 62.2 | 92.6 |
| | 800 | ✓ | ✓ | ✓ | 99.3 | 98.7 | 99.3 | 99.2 | 97.6 | 98.7 | 99.3 | 98.2 | 99.0 | 98.0 | 97.2 | 98.3 | 84.9 | 58.8 | 76.7 | 91.0 | 73.2 | 86.2 |
| Family | 200 | ✓ | ✓ | ✓ | 88.4 | 82.9 | 90.3 | 87.7 | 77.2 | 87.1 | 88.1 | 79.9 | 88.7 | 71.9 | 48.5 | 74.3 | 62.8 | 29.1 | 61.0 | 67.1 | 36.4 | 67.0 |
| | 400 | ✓ | ✓ | ✓ | 89.5 | 83.4 | 91.1 | 88.4 | 79.2 | 87.5 | 89.0 | 81.2 | 89.3 | 75.2 | 51.6 | 77.3 | 63.9 | 34.7 | 61.2 | 69.1 | 41.5 | 68.3 |
| | 600 | ✓ | ✓ | ✓ | 89.8 | 84.7 | 91.7 | 88.6 | 78.4 | 87.8 | 89.2 | 81.4 | 89.7 | 79.2 | 54.9 | 81.2 | 64.2 | 32.0 | 63.1 | 70.9 | 40.5 | 71.0 |
| | 800 | ✓ | ✓ | ✓ | 90.5 | 84.6 | 91.7 | 89.1 | 79.0 | 86.2 | 89.8 | 81.7 | 88.9 | 80.1 | 56.3 | 78.0 | 65.6 | 35.2 | 58.0 | 72.2 | 43.3 | 66.5 |
| Genus | 200 | ✓ | ✓ | ✓ | 71.0 | 48.6 | 72.8 | 71.4 | 43.0 | 68.2 | 71.2 | 45.6 | 70.4 | 52.1 | 20.6 | 53.4 | 41.8 | 8.80 | 38.5 | 46.4 | 12.3 | 44.7 |
| | 400 | ✓ | ✓ | ✓ | 72.8 | 54.5 | 75.3 | 72.6 | 40.7 | 68.2 | 72.7 | 46.6 | 71.6 | 54.4 | 25.3 | 56.3 | 43.9 | 10.7 | 40.3 | 48.6 | 15.1 | 47.0 |
| | 600 | ✓ | ✓ | ✓ | 73.4 | 56.5 | 76.5 | 73.1 | 41.6 | 68.3 | 73.2 | 47.9 | 72.2 | 54.3 | 27.1 | 56.7 | 45.5 | 10.0 | 39.1 | 49.5 | 14.6 | 46.3 |
| | 800 | ✓ | ✓ | ✓ | 74.8 | 58.5 | 76.9 | 73.4 | 43.5 | 64.0 | 74.1 | 49.9 | 69.9 | 57.0 | 30.1 | 56.2 | 46.0 | 11.7 | 35.0 | 50.9 | 16.8 | 43.2 |
| Species | 200 | ✓ | ✓ | ✓ | 55.3 | 33.5 | 58.3 | 60.4 | 17.0 | 53.9 | 57.7 | 22.6 | 56.0 | 36.4 | 10.3 | 36.9 | 27.1 | 2.80 | 22.4 | 31.0 | 4.3 | 27.9 |
| | 400 | ✓ | ✓ | ✓ | 58.1 | 38.0 | 61.8 | 61.0 | 26.5 | 55.1 | 59.5 | 31.2 | 58.3 | 37.4 | 14.9 | 40.0 | 28.3 | 3.50 | 24.1 | 32.2 | 5.7 | 30.1 |
| | 600 | ✓ | ✓ | ✓ | 58.8 | 39.7 | 62.5 | 61.9 | 27.1 | 54.3 | 60.3 | 32.2 | 58.1 | 38.1 | 15.2 | 39.6 | 29.3 | 3.20 | 23.8 | 33.1 | 5.3 | 29.7 |
| | 800 | ✓ | ✓ | ✓ | 60.4 | 42.0 | 63.7 | 62.5 | 30.1 | 50.4 | 61.4 | 35.1 | 56.2 | 40.4 | 17.4 | 40.9 | 30.4 | 3.90 | 20.3 | 34.7 | 6.4 | 27.2 |